NACA RM No. L8H05

NACA

RESEARCH MEMORANDUM

HIGH-SPEED WIND-TUNNEL TESTS OF A $\frac{1}{16}$-SCALE MODEL OF THE D-558 RESEARCH AIRPLANE - DYNAMIC PRESSURE AND COMPARISON OF POINT AND EFFECTIVE DOWNWASH AT THE TAIL OF THE D-558-1

By

Harold L. Robinson

Langley Aeronautical Laboratory
Langley Field, Va.

NATIONAL ADVISORY COMMITTEE
FOR AERONAUTICS

WASHINGTON

November 4, 1948

NACA RM No. L8H05

NATIONAL ADVISORY COMMITTEE FOR AERONAUTICS

RESEARCH MEMORANDUM

HIGH-SPEED WIND-TUNNEL TESTS OF A $\frac{1}{16}$-SCALE MODEL OF THE D-558 RESEARCH AIRPLANE - DYNAMIC PRESSURE AND COMPARISON OF POINT AND EFFECTIVE DOWNWASH AT THE TAIL OF THE D-558-1

By Harold L. Robinson

SUMMARY

Point downwash angles and the dynamic pressure at the horizontal-tail location of the D-558-1 airplane have been measured in the Langley 8-foot high-speed tunnel. The tests include a Mach number range of 0.40 to 0.94 and a lift-coefficient range of -0.3 to 0.7. Comparisons are presented with effective downwash determined from tail-on and tail-off tests.

The results indicate that the effective downwash angle, when correctly determined, agrees, within the limits of experimental accuracy, with point downwash. The downwash and velocity changes that occur at the tail location cannot cause the instability found for this airplane at low lift coefficients and at Mach numbers near 0.9. The point downwash angle at a given lift coefficient varies only slightly with Mach number; therefore, the downwash angle for level-flight lift coefficients decreases with increasing speed, and the rate of decrease with speed increases with altitude.

The rate of change of point downwash angle with lift coefficient $\left(\partial\epsilon/\partial C_L\right)$ shows a slight decrease with decreasing lift coefficient at Mach numbers above 0.9 but indicates negligible variations at other speeds. The dynamic-pressure ratio q_t/q for level-flight lift coefficients increases slightly with increasing speed.

Appendix A gives a method of correlating stability with the rate of change of downwash and dynamic pressure at the tail. Appendix B gives a method of including the effect of tail drag upon effective downwash obtained by the tail-on and tail-off method.

INTRODUCTION

There exist various methods of measuring the downwash at the tail location of an airplane model. Two of these methods, effective downwash and point downwash, were investigated to determine their applications and limitations.

Reference 1 indicated that the D-558-1 airplane had negative static longitudinal stability at low lift coefficients for a small Mach number range at approximately 0.9. The point downwash and dynamic-pressure ratio at the tail of this airplane were investigated in an attempt to ascertain their effects on the stability of this airplane.

The point downwash angles were obtained from measurements at one location with a differential pressure head (yaw head). Effective downwash angles obtained from horizontal tail-on and tail-off tests (reference 2) are shown for comparison. The dynamic pressure was obtained from static-pressure and total-pressure measurements at the horizontal-tail location.

SYMBOLS

α	angle of attack measured from airplane axis
α_y	angle between yaw-head axis and tunnel center line
α_{y_o}	angle of stream flow with respect to tunnel center line
ψ	flow angle with respect to yaw-head axis
i_y	angle between the airplane and yaw-head axes
i_t	angle of incidence of tail plane
ϵ	downwash angle
$\frac{\Delta p}{q}$	pressure-difference coefficient (yaw head)
p	standard atmospheric pressure
p_t	static pressure at tail
H_t	stagnation pressure at tail
q	free-stream dynamic pressure

[redacted]

q_t	dynamic pressure at tail
γ	ratio of specific heats (1.4)
W/S	wing loading
C_L	lift coefficient
C_m	pitching-moment coefficient about airplane center of gravity
C_{m_o}	pitching-moment coefficient at zero lift about airplane center of gravity
a_w	wing lift-curve slope
a_t	tail-plane lift-curve slope
S	wing-plan-form area
S_t	tail-plan-form area
c	mean aerodynamic chord
x	wing moment arm
l	tail moment arm
y	distance between airplane axis through center of gravity to horizontal tail plane
F, P	force vectors (see fig. 9)
m_t	pitching moment about tail caused by forces on tail plane
ΔM	pitching moment about airplane center of gravity caused by forces on tail plane

Subscripts 0, 1, and 2 refer to specific values as defined in paper.

APPARATUS

The downwash-angle and dynamic-pressure investigation was conducted in the Langley 8-foot high-speed tunnel which is a single-return, closed-throat tunnel. The maximum corrected Mach number reported for this investigation was about 0.94. The Reynolds number varied from about 1×10^6 to 1.6×10^6.

[redacted]

Model.- The metal model was constructed by the NACA and is described in references 1, 2, and 3. The complete model, without the stabilizer, was used for this series of tests. A three-view drawing of the model is presented as figure 1.

Yaw-head and pressure-measuring instruments.- The point downwash was measured with a small yaw head mounted at the 50-percent-chordwise station, at the left midsemispan of the stabilizer (fig. 1). The yaw head was mounted on the sting which supported the model in the tunnel. Thus, when the model angle of attack was changed, the yaw head remained fixed with relation to the model. This yaw head is the same one that was used in reference 4. A total-head tube was mounted between the yaw-head tubes in order to obtain the total pressures. A static-pressure tube was mounted on the right side of the model, symmetrically with the yaw head.

TESTS AND REDUCTION OF DATA

The yaw head was calibrated at the test Mach numbers by measuring the pressures at the open ends of the tubes with the yaw head rotated at various angles with respect to the tunnel axis. The pressures were measured with the yaw head in the normal position and the inverted position. (The inverted position was obtained by rotating the yaw head 180° about its axis.) This method of calibration, which is the same as that used in reference 4, eliminates the error due to stream misalinement in the tunnel.

This calibration method can be further explained by referring to figure 2. The angle between the yaw-head axis and the tunnel center line is α_y and the average curve represents the pressure difference that would have been measured with a perfectly machined yaw head. Therefore, the flow for this illustration is inclined upwards α_{y_o} degrees (negative) with respect to the tunnel axis, and the flow direction with respect to the yaw head is given by

$$\psi = \alpha_y - \alpha_{y_o}$$

Therefore, when a pressure-difference coefficient of $\left(\frac{\Delta p}{q}\right)_1$ is measured at the tail plane with the yaw head in the upright position, the flow direction with respect to the yaw head is the angle ψ_1, not α_{y_1}. The point downwash angle is given by

$$\epsilon = \alpha + i_y - \psi \qquad (1)$$

[redacted]

where α is the corrected angle of attack of the model and i_y is the angle between the model center line and the yaw-head axis, taken as positive clockwise from the model center line when the model is viewed from the left. Furthermore it was found that the calibration of the yaw head remained constant with changes in free-stream Mach number.

The total-head tube between the two tubes of the yaw head, and the static-pressure tube were calibrated at the same time the yaw head was calibrated, and it was found that no error was introduced by the flow being slightly inclined with respect to the total-head or the static-pressure tubes. The dynamic pressures at the tail were obtained by measuring the static pressure p_t and the total pressure H_t at the horizontal-tail location. The dynamic pressure at the tail was then calculated from

$$q_t = H_t \frac{\gamma}{\gamma - 1} \left[\left(\frac{p_t}{H_t} \right)^{1/\gamma} - \frac{p_t}{H_t} \right] \tag{2}$$

where γ is the ratio of specific heats for air and is equal to 1.4.

The jet-boundary, constriction, and wake-blockage corrections that were applied to Mach number, lift coefficient, and free-stream dynamic pressure in reference 1 were applied to these data. The magnitude of the downwash angle depends on the sum of three angles whose individual measurements are accurate to 0.1°. The total error for the downwash angle ϵ may therefore be as large as 0.3°. Jet-boundary corrections have not been applied to the downwash-angle data. These jet-boundary corrections are usually smaller than 0.3°.

RESULTS AND DISCUSSION

The variation of point downwash with lift coefficient is presented in figure 3. The point downwash is also compared with the effective downwash obtained from reference 2.

The point downwash and effective downwash are in agreement within the experimental accuracy of the data at Mach numbers below 0.875. The discrepancy which was as large as 3° at higher speeds is partly attributable to the method used in computing the effective downwash, in which the airplane pitching moment due to the drag of the stabilizer was assumed to be of negligible consequence. While the drag of the tail has little effect at the lower speeds, it has a sizeable effect on the effective downwash values determined by this method at the higher speeds, especially if the critical speed of the tail plane has been exceeded. A correction for this drag effect

is given in appendix B. The data were recomputed, using this method, for Mach numbers of 0.6 and 0.933. There was no significant change in the values reported in reference 2 at a Mach number of 0.6, but the values of the downwash angles were reduced about 1° at a Mach number of 0.933 (fig. 3). The data obtained by the corrected method, however, are still subject to the errors inherent in the graphical procedure.

Furthermore the method for obtaining effective downwash in reference 2 does not consider any interference effects which exist at the fin-stabilizer juncture. The flow at the under side of the stabilizer at the juncture may be accelerated because of the fin stabilizer and fuselage juxtaposition. This consideration would effectively give the stabilizer negative aerodynamic camber which would increase the stabilizer angle of zero lift. Tests of the model without the wing and with and without the stabilizer indicate that the apparent zero-lift angle of the tail is approximately 1.7° at low Mach numbers and that the zero-lift angle at a Mach number of 0.93 is approximately 1.5° higher than the zero-lift angle at low speeds (fig. 4). The downwash angle, as indicated by the point-downwash method, is also 1.7° at zero lift (fig. 3). It is concluded that the flow at the tail is influenced by the rudder and fuselage shape to cause a downwash of 1.7° at zero lift. The increase of zero-lift angle with Mach number, if taken into account for the effective-downwash measurement, consequently would reduce the value from reference 2 by 1.5° at a Mach number of 0.93. Figure 3 indicates that the downwash angles given by the point-downwash method and effective-downwash method may be in fair agreement when the tail drag and interference are considered.

The effective downwash angle represents a mean value, and since the point downwash angle represents the value at a specific point, the difference between the point downwash and the corrected effective downwash may give an indication of the spanwise variation of the downwash at the tail. When the effective downwash is equal to the point downwash, there may or may not be a spanwise variation of downwash; but when there is a difference between the effective downwash and point downwash, a variation in the magnitude of the downwash angle at different spanwise stations of the tail exists. These tests, however, do not indicate that a spanwise variation exists. It may be concluded that the effective downwash is not a measure of the actual flow direction at a given point at the tail location at high speeds, and the point downwash cannot be utilized to indicate control settings required to trim without consideration of the spanwise distribution of point downwash.

The point-downwash data presented in reference 4 indicated an increase in downwash angle with Mach number at a given lift coefficient beyond the force-break Mach number of the wing. These data are not directly comparable to the data in this paper since the wing aspect ratio is smaller and the location of the tail is higher for the

D-558-1 airplane than for the configurations investigated in reference 4. Furthermore, the data in reference 4 indicated that as the height of the tail was increased, the effect of Mach number on downwash angle was diminished. The data in reference 4 therefore are not in disagreement with the point-downwash data presented in this paper.

Figure 3 indicates that the point downwash increases with lift coefficient; that there is very little change with Mach number at a given lift coefficient; and that the variation of the rate of change of point downwash $\partial\epsilon/\partial C_L$ may cause a stabilizing effect at low lift coefficients and high Mach numbers for the D-558-1 airplane. Therefore, the change of $\partial\epsilon/\partial C_L$ does not account for the unstable tendency reported in reference 1. Furthermore, the effective-downwash data of reference 2 indicated similar effects in several instances.

The point downwash angles at level-flight lift coefficients are presented as a function of free-stream Mach number in figure 5. The level-flight lift coefficients were computed from

$$C_L = \frac{2}{\gamma p M^2} \frac{W}{S} \tag{3}$$

where the wing loading W/S is 58 pounds per square foot, p is the standard pressure at the altitude for which the computations are made, M is Mach number, and γ is the ratio of specific heats for air and is equal to 1.4. Thus the point downwash angle at a given Mach number and computed lift coefficients are obtained from figure 3 and plotted as a function of Mach number and altitude in figure 5. This figure indicates that the point downwash angle decreases as the airplane speed increases, and the rate of decrease of downwash angle with speed will increase with increasing altitude.

The variation with Mach number of the rate of change of point downwash with lift coefficient $\partial\epsilon/\partial C_L$ at level-flight lift coefficients is presented in figure 6 and is obtained by measuring the slopes of the curves of figure 3 at the computed level-flight lift coefficient for a given Mach number and altitude. This figure (fig. 6) indicates that at level-flight lift coefficients $\partial\epsilon/\partial C_L$ remains nearly constant up to a Mach number of 0.85 (approximate) and then decreases approximately from 5 to a value of 4 at a Mach number of 0.933, the highest Mach number reported.

The relationship between incremental rate of change of downwash $\Delta\frac{\partial\epsilon}{\partial C_L}$ and incremental stability $\left(\Delta\frac{\partial C_m}{\partial C_L}\right)_\epsilon$ due to downwash changes is developed in appendix A. It is indicated that when $\partial\epsilon/\partial C_L$

[redacted]

decreases 1.0, at a Mach number of 0.933 the stability parameter $\partial C_m/\partial C_L$ consequently will decrease approximately 0.04. Thus, there is a tendency to increase the stability of the airplane by 0.04 at the highest Mach number reported (0.933). It should be remembered, however, that point-downwash changes cannot be utilized to estimate stability changes accurately unless the spanwise distribution of downwash is taken into account. The foregoing values are presented merely to indicate the relative order of magnitude of $d\epsilon/dC_L$ increments and stability increments.

The dynamic pressures measured at the tail are presented in figure 7 as a function of lift coefficient at various values of the corrected free-stream Mach number. A cross plot presenting the dynamic-pressure ratio as a function of Mach number and lift coefficient is presented in figure 8. This figure indicates that the dynamic-pressure ratio is approximately equal to unity, for the lift-coefficient range measured, up to a Mach number of approximately 0.75. Above a Mach number of 0.875, the dynamic-pressure ratio at a given Mach number varies inversely with lift coefficient. The relation between incremental dynamic-pressure ratio $\Delta\frac{q_t}{q}$ and incremental stability $\left(\Delta\frac{\partial C_m}{\partial C_L}\right)_q$ is developed in appendix A. Figure 8 and equation (A4) indicate that the measured dynamic-pressure-ratio changes have a small effect on the static longitudinal stability of the D-558-1 airplane. The variation of dynamic-pressure ratio with Mach number at level-flight lift coefficient (fig. 9) indicates that the maximum increase in dynamic-pressure ratio is approximately 0.03 at a Mach number of 0.9. Equation (A4) indicates that this would cause the airplane static-longitudinal-stability parameter $\partial C_m/\partial C_L$ to decrease approximately 0.007, making the airplane more stable by this amount. It should be remembered that appendix A indicated that the two effects cannot be added to obtain the total-stability change.

CONCLUSIONS

Measurements of point downwash and dynamic pressure at the stabilizer location of the D-558-1 airplane indicate that:

1. Effective downwash determined from the tail-on and tail-off tests differs from the values obtained by the point-downwash method by as much as 3°; however, effective downwash agrees, within the limits of experimental accuracy, with point downwash, if the effective-downwash determination includes a consideration of tail drag and fin-stabilizer-fuselage interference. The spanwise variation of point downwash at the tail should be considered to determine the effect of downwash on trim configurations.

2. The flow direction at the tail is influenced by the fuselage and rudder shape; furthermore, the coincidence of zero downwash and zero lift is not a necessary consequence.

3. The rate of change of downwash angle with lift coefficient does not change through the lift-coefficient and Mach number ranges investigated in a manner which would produce the decrease of static longitudinal stability which exists for this airplane for a small lift-coefficient and Mach number range. Rather, a tendency to increase the static longitudinal stability at low lift coefficients and higher speeds occurs.

4. At level-flight lift coefficients, the point downwash angle decreases with increasing speed, and the rate of decrease with speed increases with altitude. There were no abrupt downwash changes due to increasing Mach number.

5. The dynamic-pressure changes that occur at the horizontal tail of the D-558-1 airplane, within the range of this investigation, are not sufficient to affect the static longitudinal stability of this airplane seriously.

Langley Aeronautical Laboratory
National Advisory Committee for Aeronautics
Langley Field, Va.

[redacted]

APPENDIX A

THE EFFECT OF THE RATE OF CHANGE OF DOWNWASH WITH LIFT COEFFICIENT, AND OF THE DYNAMIC-PRESSURE RATIO ON STATIC LONGITUDINAL STABILITY

The effect of changes in the rate of change of downwash angle $\partial\epsilon/\partial C_L$ and dynamic-pressure ratio q_t/q on the static longitudinal stability characteristics has been calculated by the equations developed in this appendix.

Neglecting the contribution of the tail plane to the total airplane lift, all drag and thrust components, and all lift and moment components except those due to the wing and stabilizer, the pitching-moment coefficient can be written in the familiar simplified form:

$$C_m = \alpha a_w \frac{x}{c} + C_{m_o} - (\alpha + i_t - \epsilon)\, a_t \frac{q_t}{q} \frac{S_t}{S} \frac{l}{c} \tag{A1}$$

where a is the lift-curve slope; x is the horizontal distance from the wing aerodynamic center to the airplane center of gravity taken as positive when the aerodynamic center is ahead of the center of gravity; c is the wing mean aerodynamic chord; S is the plan-form area; l is the tail moment arm; and subscripts w and t refer to the wing and horizontal tail plane, respectively. The familiar simplified form of the stability equation is:

$$\frac{\partial C_m}{\partial C_L} = \frac{x}{c} - \left(\frac{1}{a_w} - \frac{\partial\epsilon}{\partial C_L}\right) a_t \frac{q_t}{q} \frac{S_t}{S} \frac{l}{c} \tag{A2}$$

The incremental stability due to changes only in the rate of variation of downwash angle with lift coefficient is

$$\left(\Delta\frac{\partial C_m}{\partial C_L}\right)_\epsilon = \Delta\frac{\partial\epsilon}{\partial C_L}\, a_t \frac{S_t}{S} \frac{l}{c} \frac{q_t}{q} \tag{A3}$$

[redacted]

and the incremental stability due to dynamic-pressure-ratio changes only is

$$\left(\Delta\frac{\partial C_m}{\partial C_L}\right)_q = -\Delta\frac{q_t}{q}\frac{S_t}{S}\frac{l}{c}\left(\frac{1}{a_w}-\frac{\partial\epsilon}{\partial C_L}\right)a_t \qquad (A4)$$

The tail volume coefficient $\frac{S_t}{S}\frac{l}{c}$ of the D-558-1 airplane is 0.667. The value of a_w to be used in equation (A4) may be obtained from reference 3 where it is given as 0.09 at a Mach number of 0.9. The value of a_t to be used with equations (A3) and (A4) is about 0.06. This value of a_t was obtained from tests without the stabilizer and with the stabilizer set at various incidence angles both without the wing.

It should be emphasized that adding the separate effects of equations (A3) and (A4) does not give the complete stability change since the term involving the product of the increments is not included. However, this product term is usually small.

[redacted]

APPENDIX B

A METHOD OF OBTAINING DOWNWASH FROM TESTS OF AN AIRPLANE MODEL WITH AND WITHOUT THE HORIZONTAL TAIL

The forces on a horizontal tail may be specified by force vectors F and P and the couple m_t (fig. 10). The force vectors F and P are perpendicular and parallel to the stream direction. However, instead of the vectors F and P, we may use vectors F_1 and P_1 perpendicular and parallel to the tail plane, or F_2 and P_2 perpendicular and parallel to the airplane axis.

The following relationships may be established from the geometry of figure 10:

$$F_1 = F \cos \left(\alpha + i_t\right) + P \sin \left(\alpha + i_t\right) \tag{B1}$$

$$\left.\begin{aligned} F_2 &= F \cos \alpha + P \sin \alpha \\ P_2 &= P \cos \alpha - F \sin \alpha \end{aligned}\right\} \tag{B2}$$

$$\Delta M = yP_2 - lF_2 + m_t \tag{B3}$$

When the angle of attack of the symmetrical tail section is zero,

$$\epsilon = \alpha + i_t$$

$$F_1 = 0$$

$$m_t = 0$$

and, from equation (B1), for $F_1 = 0$

$$F = -P \tan \left(\alpha + i_t\right) \tag{B4}$$

Substituting equation (B4) in equations (B2),

$$\left.\begin{aligned} F_2 &= P \left[\sin \alpha - \tan \left(\alpha + i_t\right) \cos \alpha\right] \\ P_2 &= P \left[\cos \alpha + \tan \left(\alpha + i_t\right) \sin \alpha\right] \end{aligned}\right\} \tag{B5}$$

Substituting equations (B5) in equation (B3),

$$\begin{aligned} \Delta M = {} & yP \left[\cos \alpha + \tan \left(\alpha + i_t\right) \sin \alpha\right] \\ & - lP \left[\sin \alpha - \tan \left(\alpha + i_t\right) \cos \alpha\right] \end{aligned}$$

which can be simplified to

$$\Delta M = P \left(y \cos i_t + l \sin i_t\right) \sec \left(\alpha + i_t\right) \tag{B6}$$

But,

$$\cos \left(\alpha + i_t\right) = 1 - \left(\frac{\pi}{180}\right)^2 \frac{\left(\alpha + i_t\right)^2}{2!} + \ldots$$

$$\cos i_t = 1 - \left(\frac{\pi}{180}\right)^2 \frac{i_t^2}{2!} + \ldots$$

$$\sin i_t = \frac{\pi}{180} i_t - \left(\frac{\pi}{180}\right)^3 \frac{i_t^3}{3!} + \ldots$$

where angles are given in degrees. Thus, for small values of α and i_t, equation (B6) reduces to

$$\Delta M = P \left(y + \frac{\pi}{180} l i_t\right) \tag{B7}$$

[redacted]

Writing equation (B7) in coefficient form gives

$$\Delta C_m = \Delta C_D \left(\frac{y}{c} + \frac{\pi}{180} \frac{l}{c} i_t \right) \tag{B8}$$

Since $\frac{y}{c} = 0.51$ and $\frac{l}{c} = 2.39$ for the D-558-1 airplane,

$$\Delta C_m = \Delta C_D \left(0.51 + 0.0417 \, i_t \right) \equiv \Delta C_D \, f(i_t) \tag{B9}$$

for $F_1 = 0$. The downwash angle is given by

where

$$\left.\begin{aligned} \epsilon &= \alpha + i_t \\ \Delta C_m &= \Delta C_D \, f(i_t) \end{aligned}\right\} \tag{B10}$$

Thus, if the tail-moment increment from test data is plotted against i_t for a constant α and Mach number, and if equation (B9) is plotted on the same coordinates, the intersection will give a value of α and i_t whose sum is equal to the downwash angle. It will be of some help to note that while ΔC_D is a function of α, i_t, and Mach number, it may be assumed that its variation with α and i_t is small enough to be ignored in many practical examples.

[redacted]

REFERENCES

1. Wright, John B.: High-Speed Wind-Tunnel Tests of a $\frac{1}{16}$-Scale Model of the D-558 Research Airplane. Basic Longitudinal Stability of the D-558-1. NACA RM No. L7K24, 1948.

2. Wright, John B.: High-Speed Wind-Tunnel Tests of a $\frac{1}{16}$-Scale Model of the D-558 Research Airplane. Longitudinal Stability and Control of the D-558-1. NACA RM No. L8C23, 1948.

3. Wright, John B., and Loving, Donald L.: High-Speed Wind-Tunnel Tests of a 1/16-Scale Model of the D-558 Research Airplane. Lift and Drag Characteristics of the D-558-1 and Various Wing and Tail Configurations. NACA RM No. L6J09, 1946.

4. Whitcomb, Richard T.: An Investigation of the Downwash behind a High-Aspect-Ratio Wing with Various Amounts of Sweep in the Langley 8-Foot High-Speed Tunnel. NACA RM No. L8C12, 1948.

[redacted]

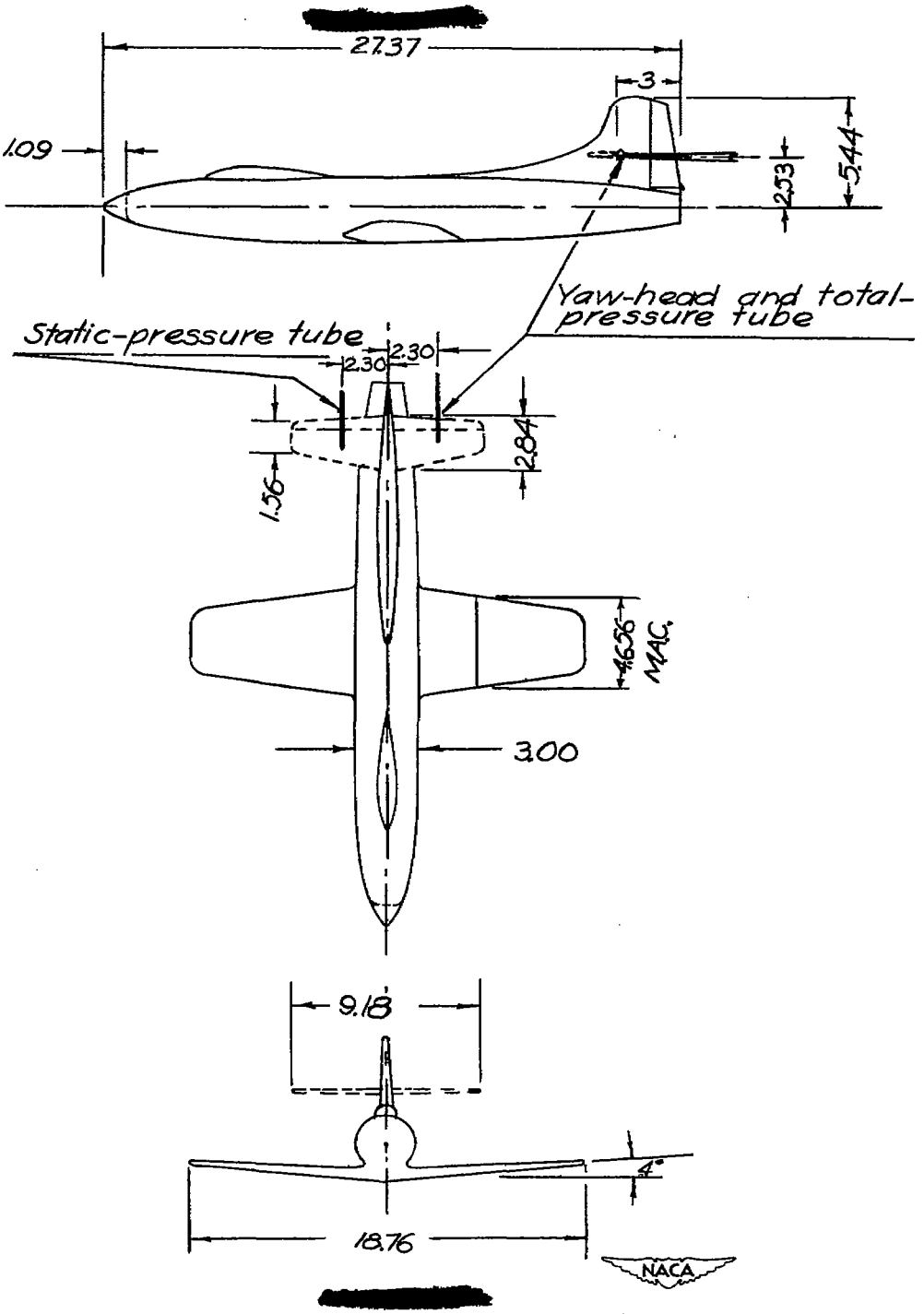

Figure 1 .- Drawing of the $\frac{1}{16}$-scale D-558-1 model showing the location of the downwash measuring apparatus. All dimensions in inches.

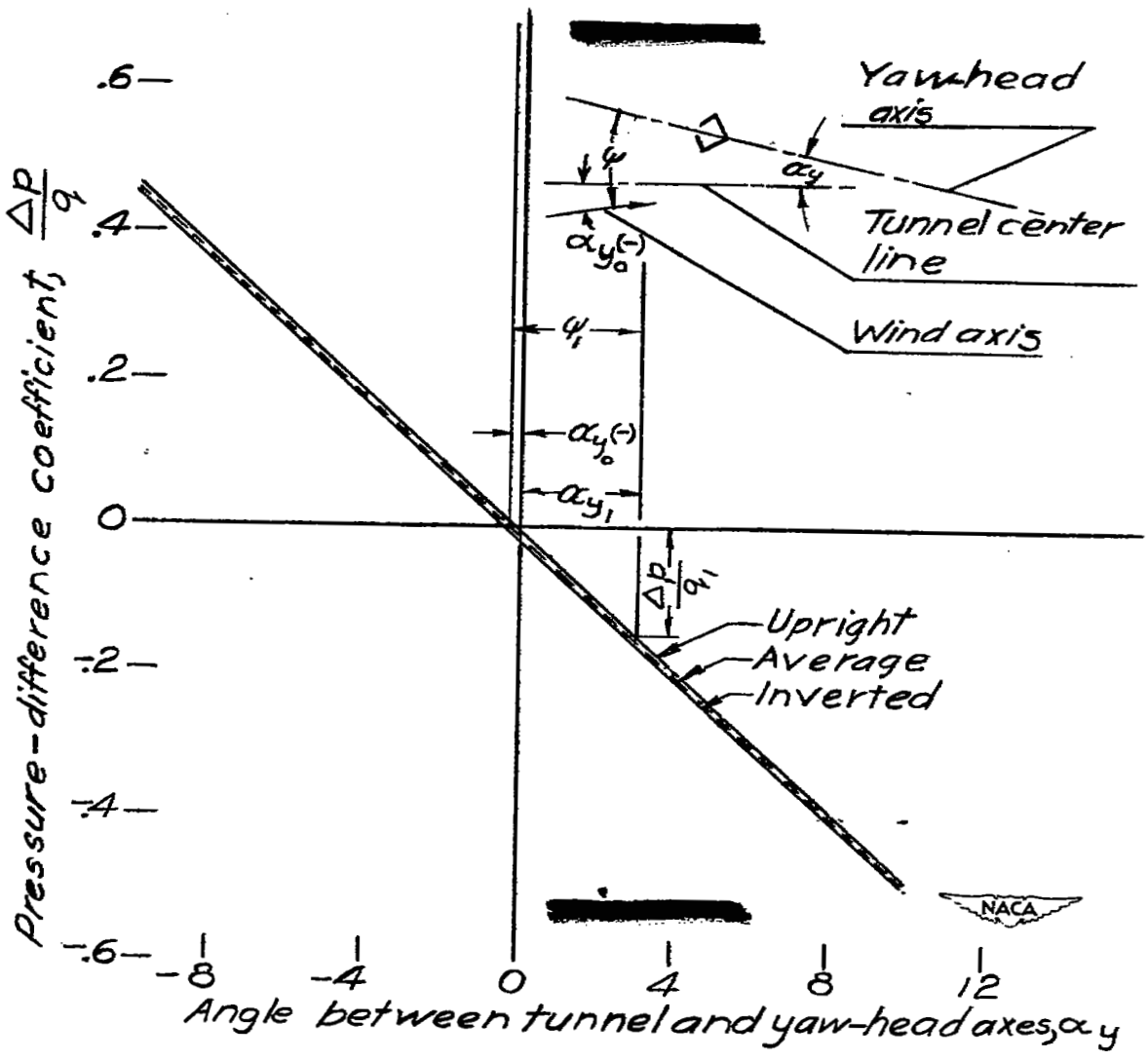

Figure 2.- Sample yaw-head calibration curve.

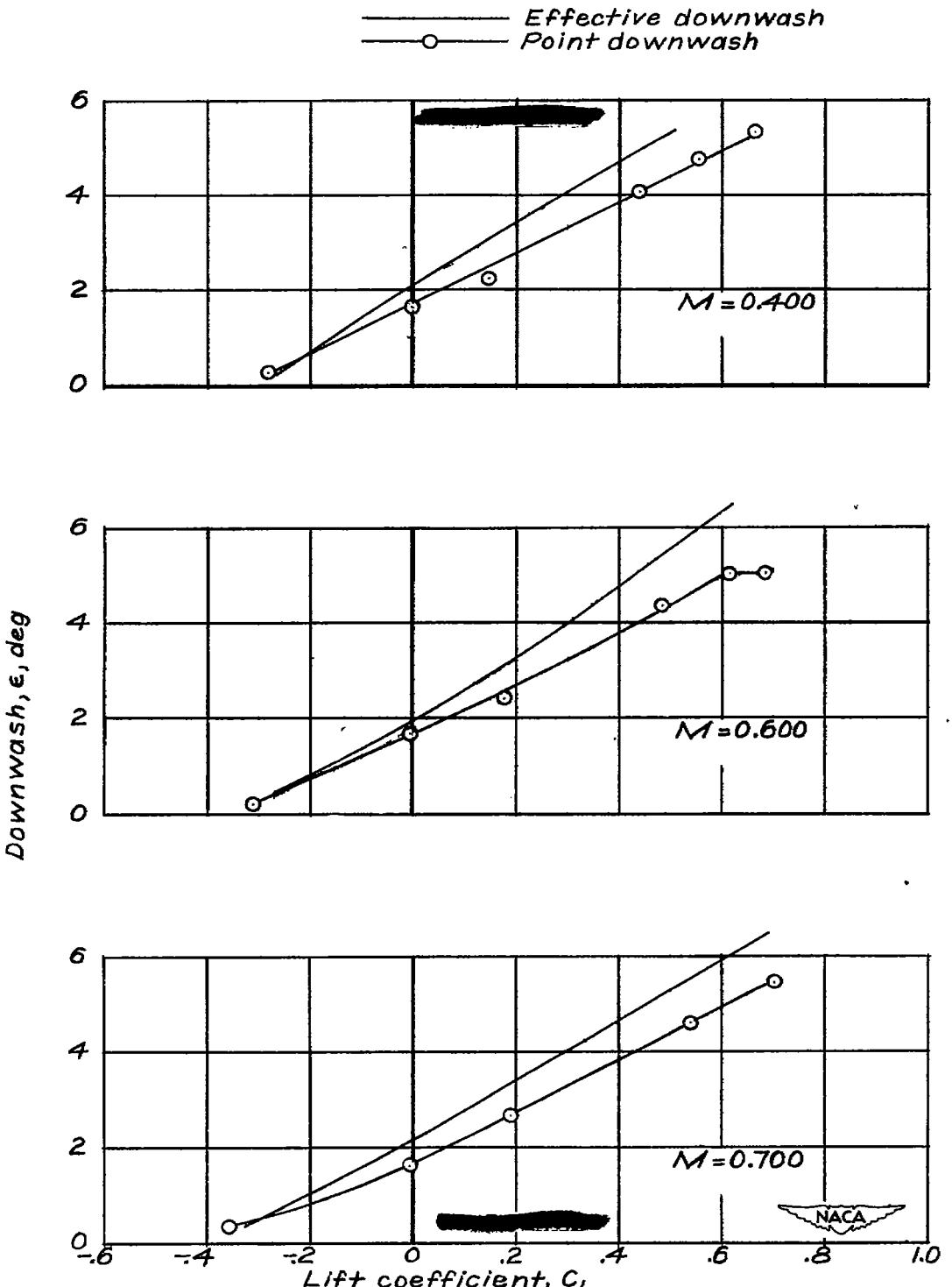

Figure 3 .- Comparison of effective downwash with point downwash.

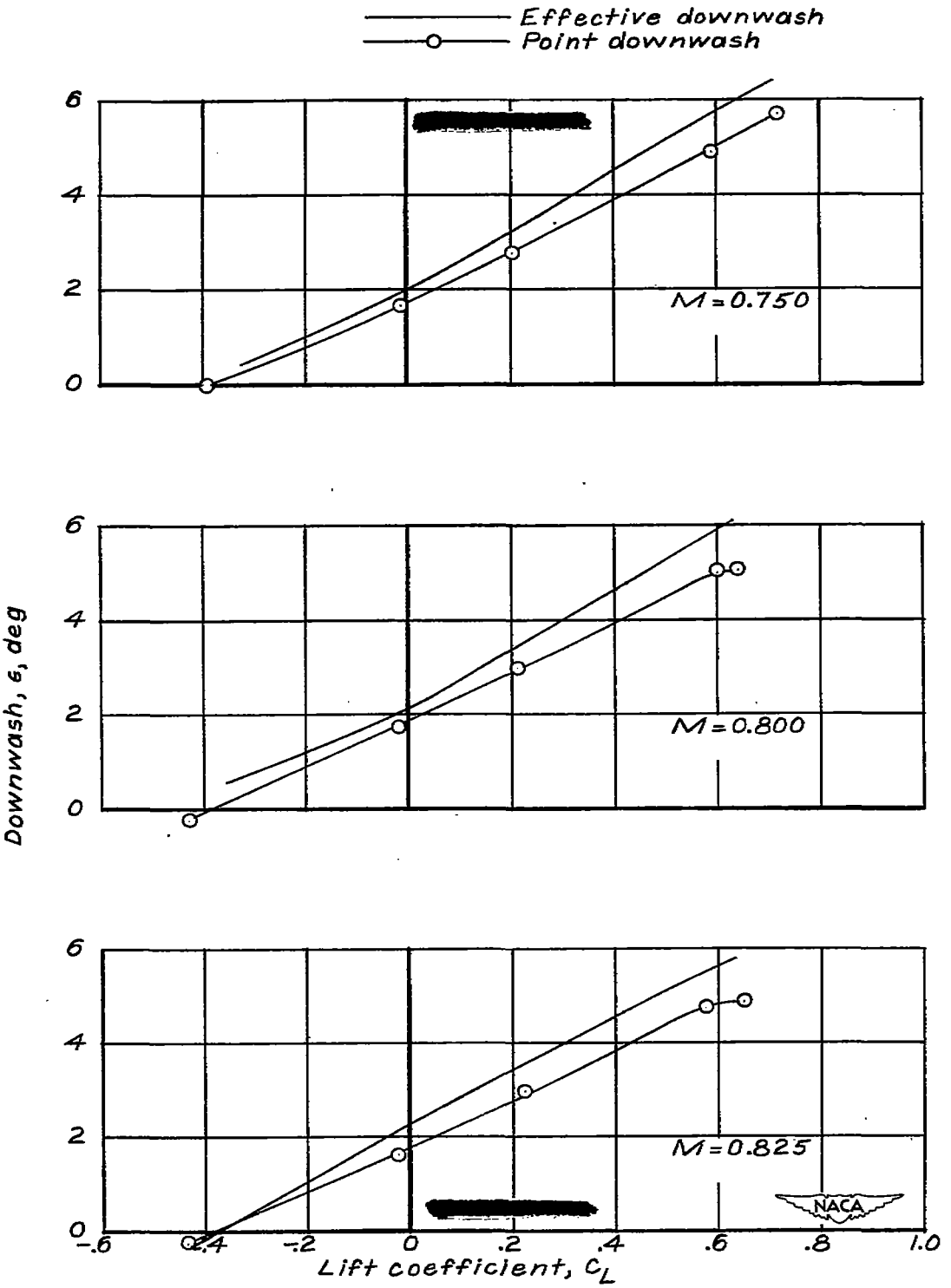

Figure 3 .- Continued.

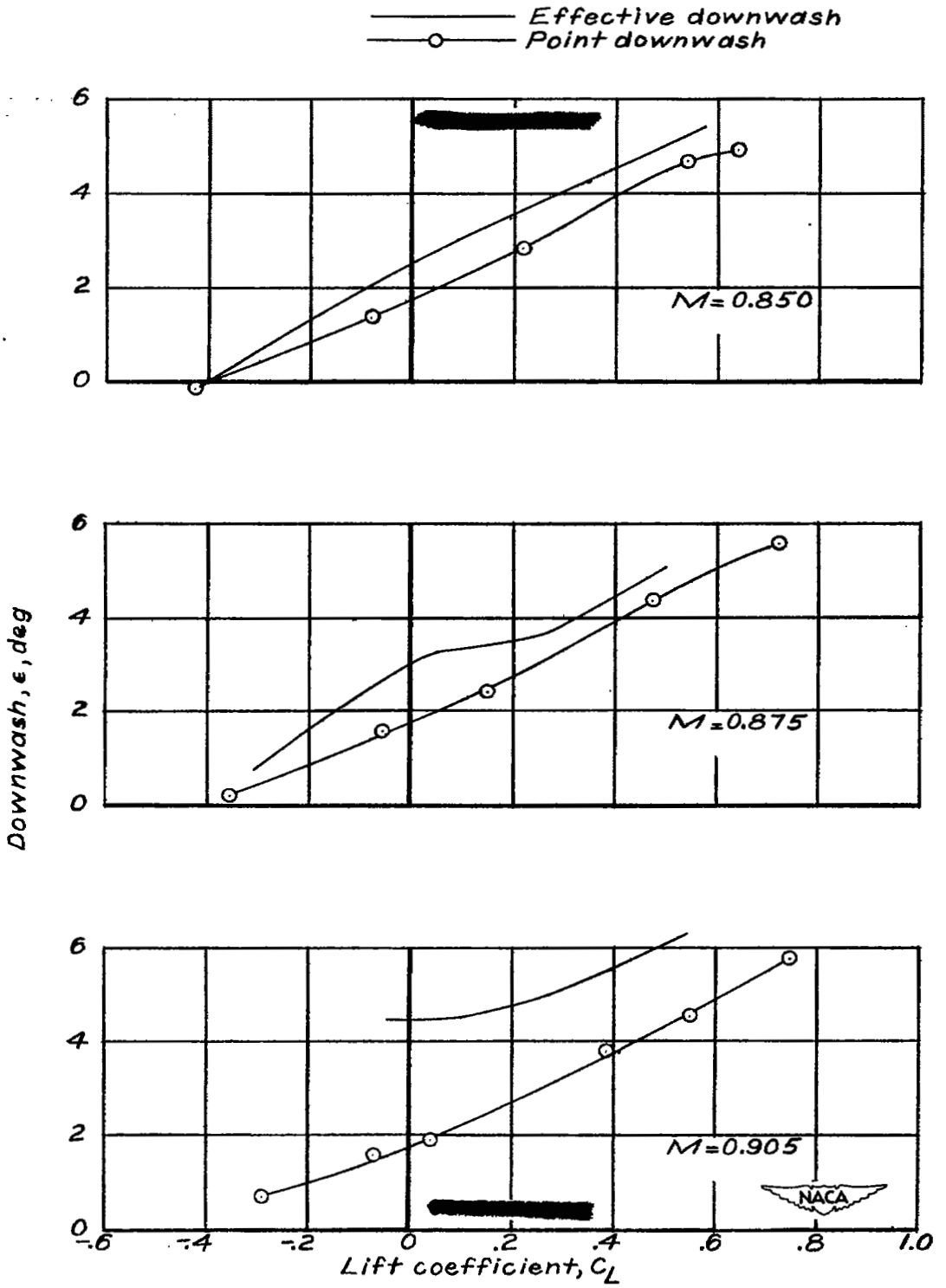

Figure 3.- Continued.

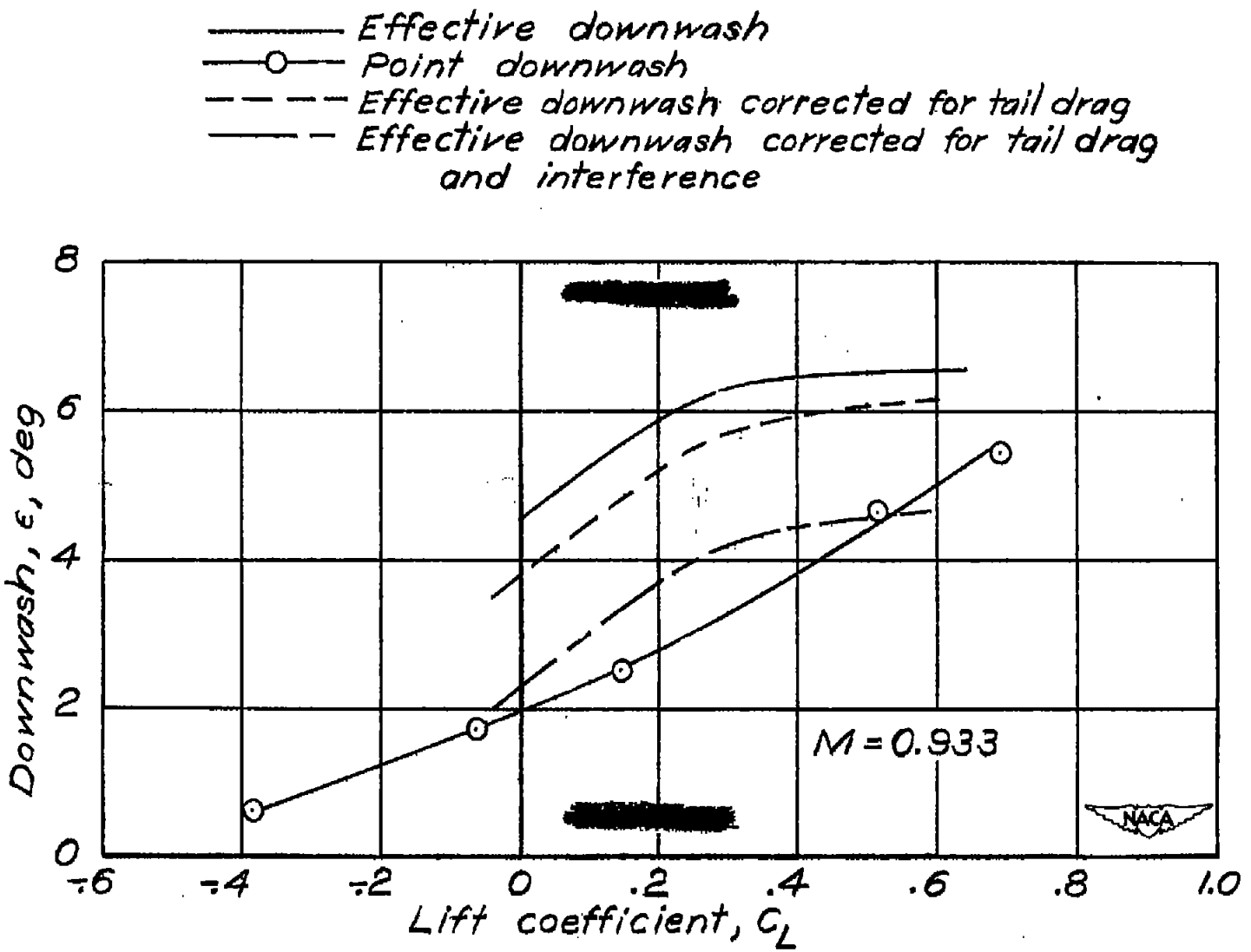

Figure 3.- Concluded.

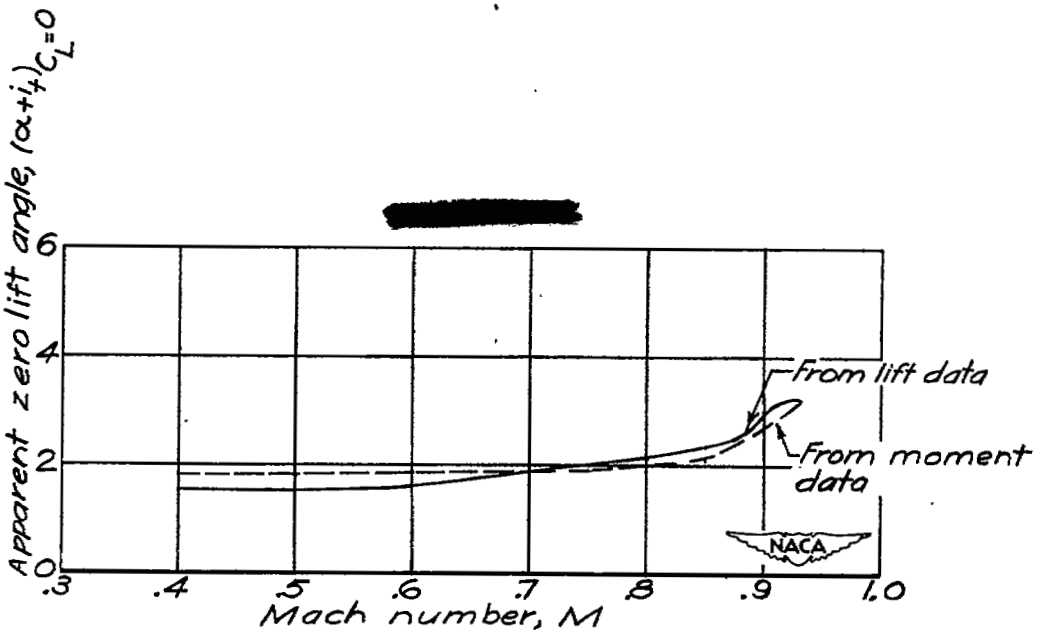

Figure 4.- Apparent zero lift angle for the horizontal tail.

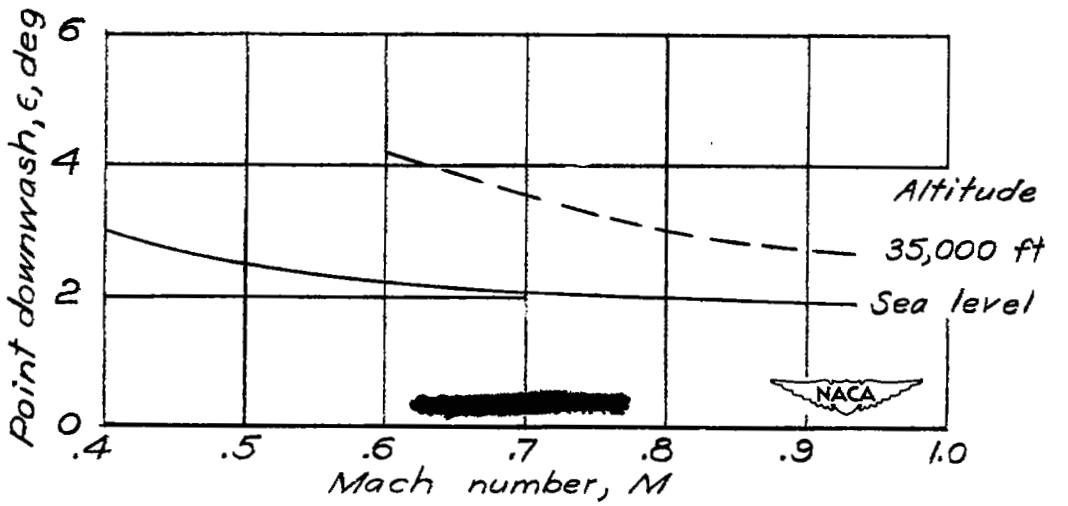

Figure 5.- Variation of downwash with Mach number at level-flight lift coefficients for wing loading of 58 pounds per square foot.

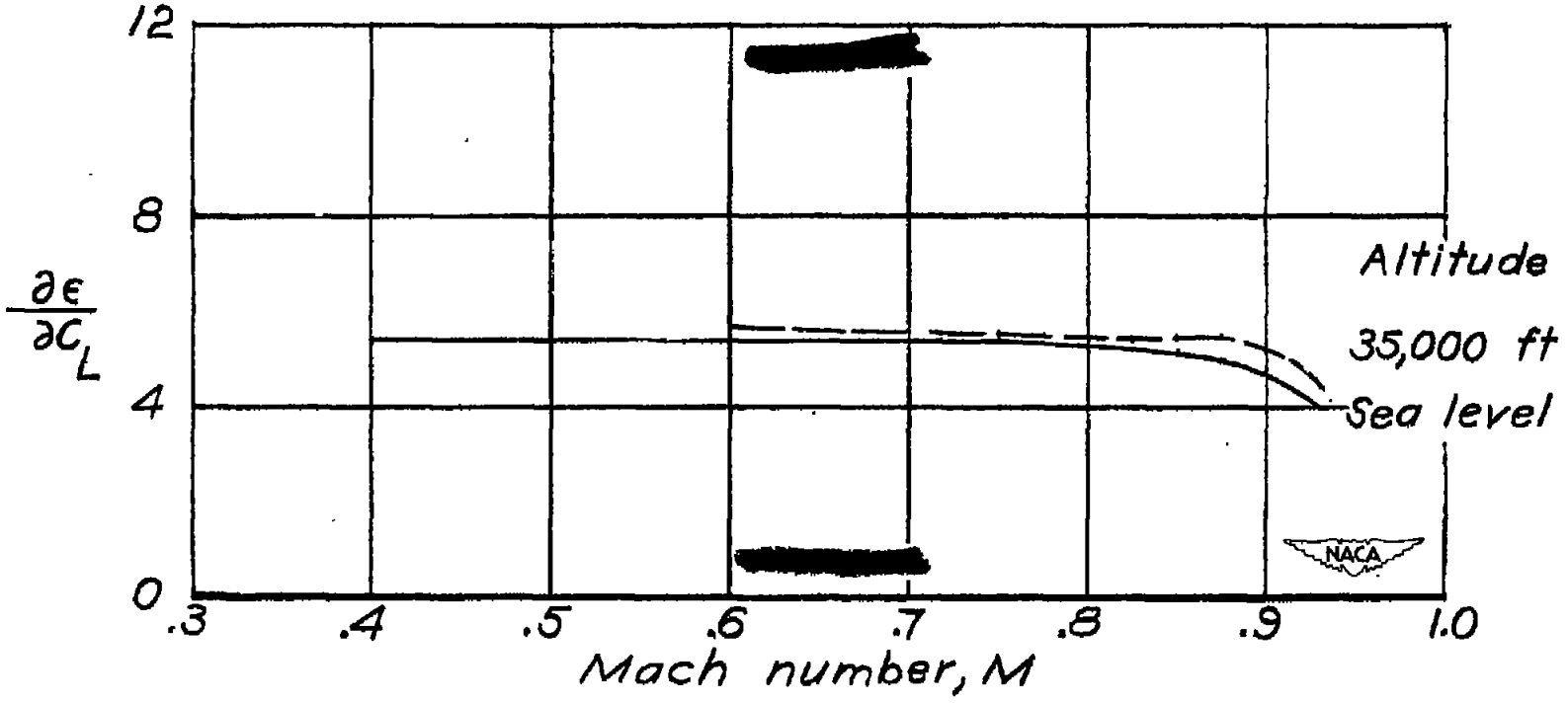

Figure 6.- Variation of the rate of change of point downwash with Mach number at level-flight lift coefficients.

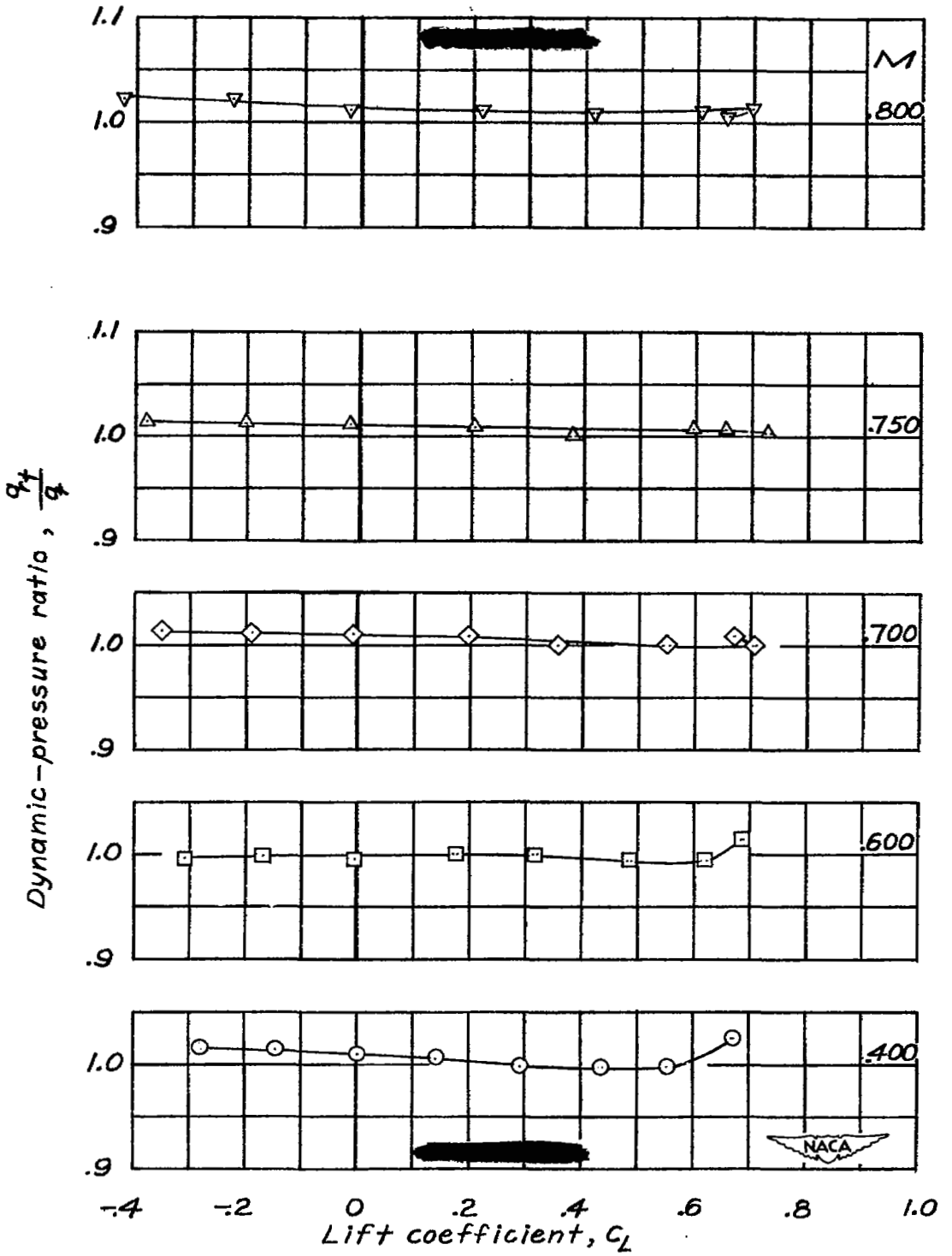

Figure 7 .-Variation of dynamic-pressure ratio with lift coefficient at various Mach numbers.

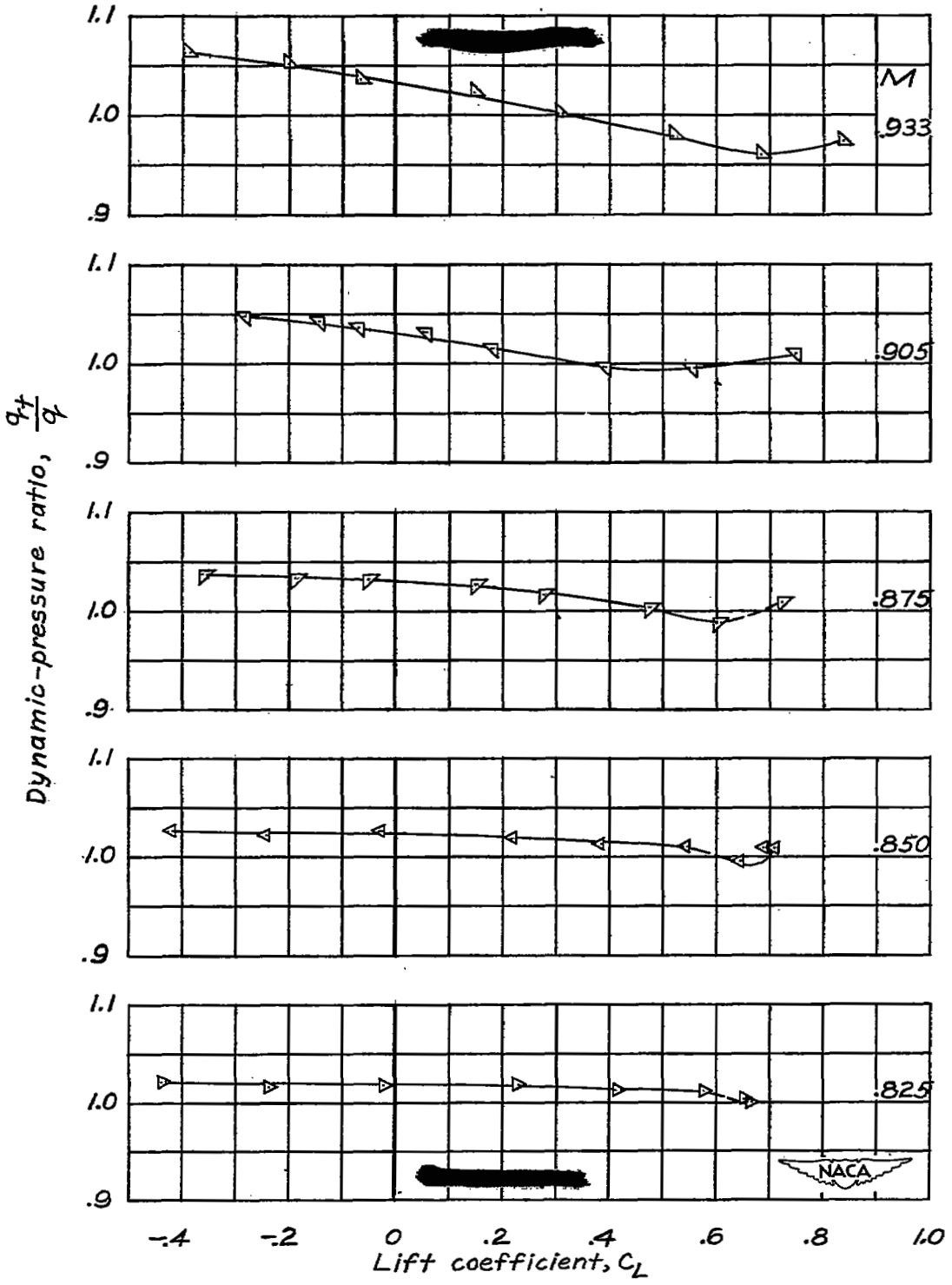

Figure 7 .- Concluded.

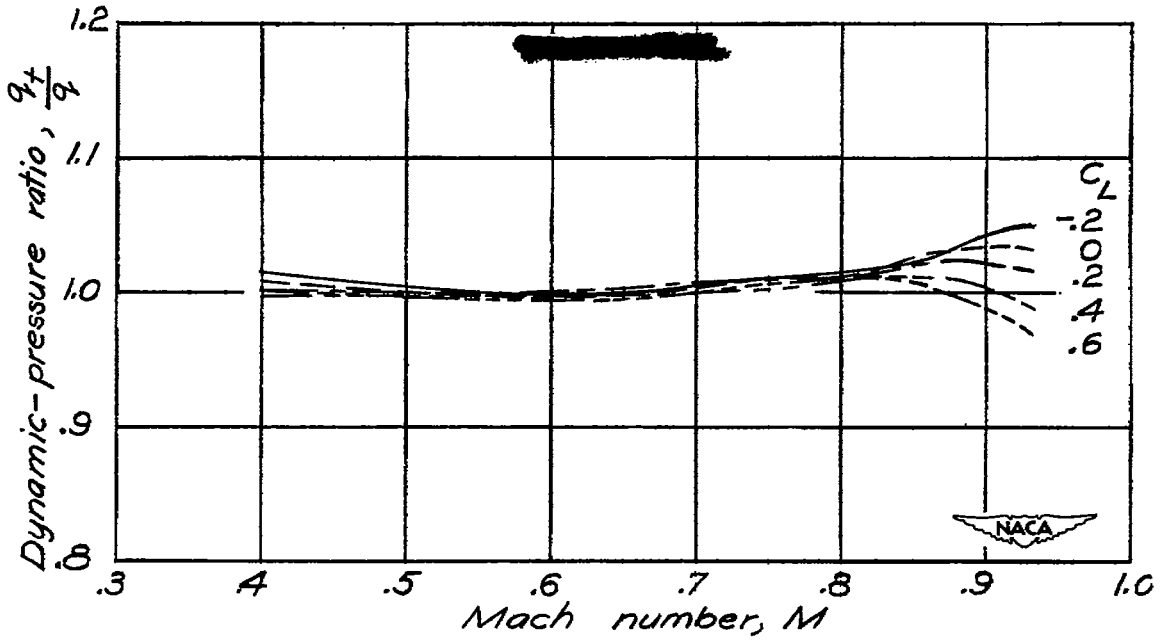

Figure 8 .- Variation of dynamic-pressure ratio with Mach number at various constant lift coefficients.

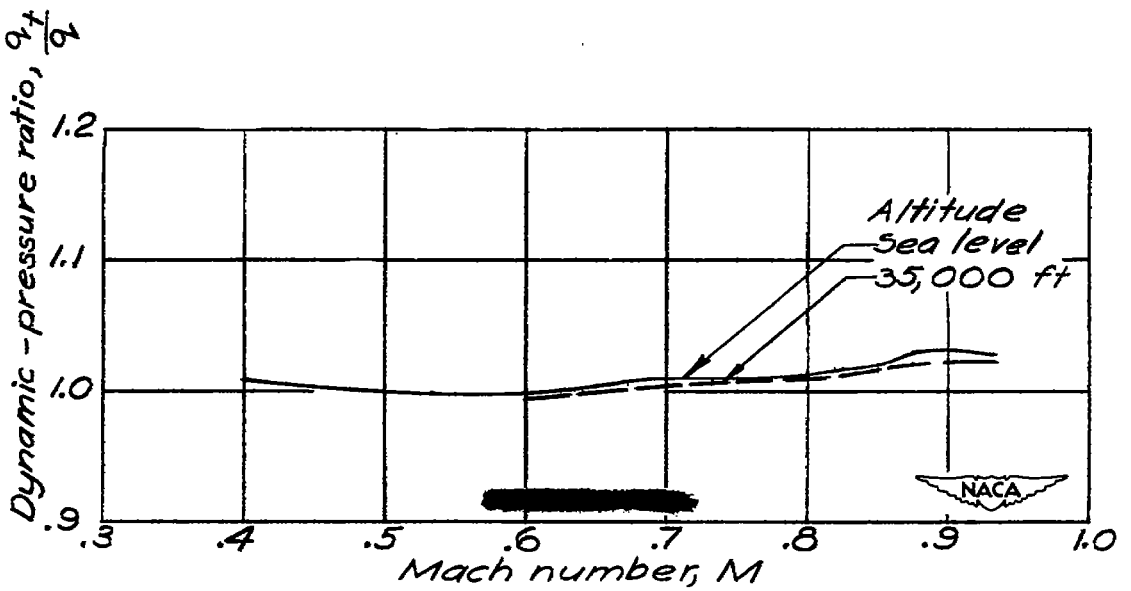

Figure 9.- Variation of dynamic-pressure ratio with Mach number for level-flight lift coefficients.

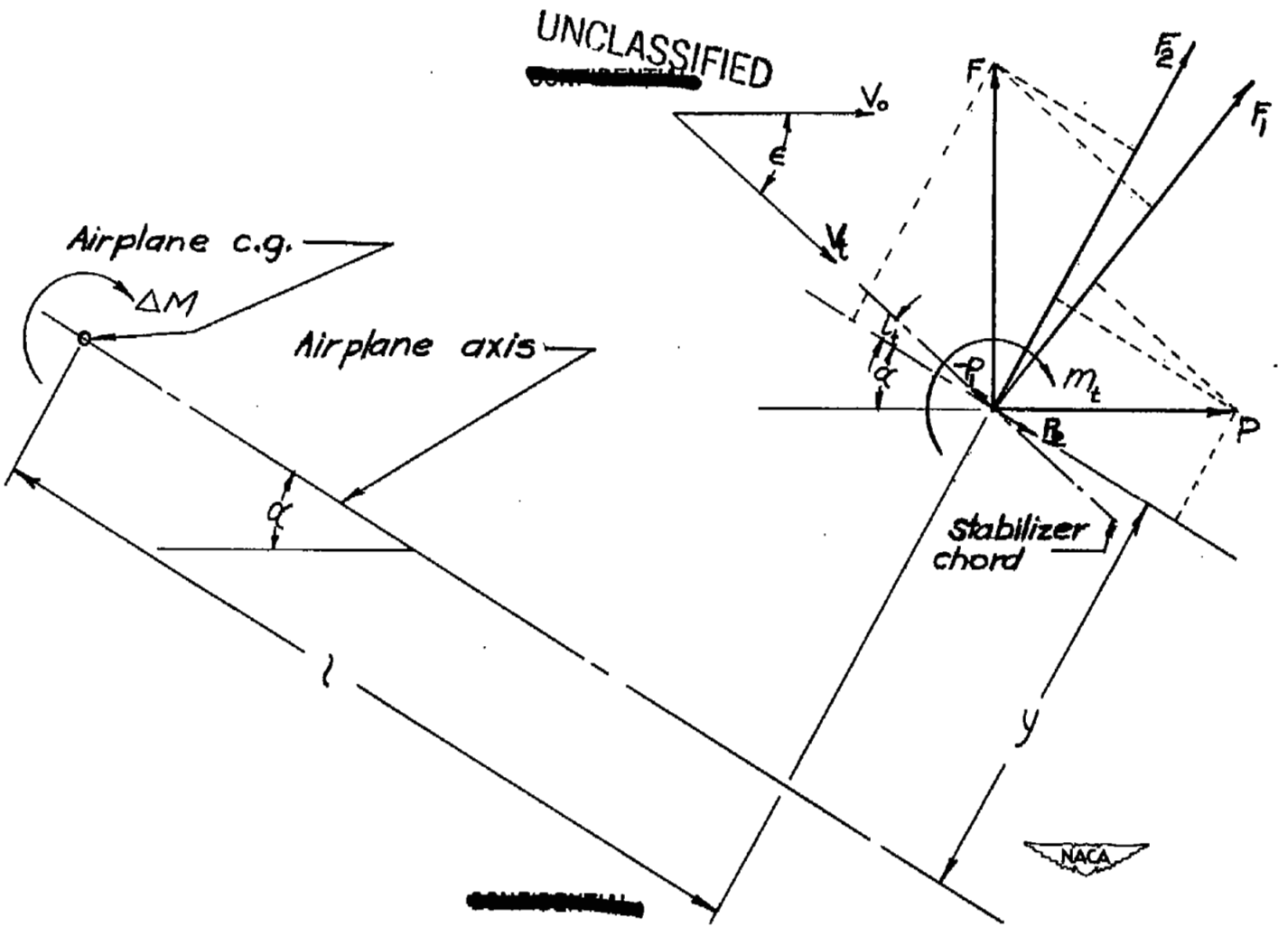

Figure 10.- Schematic diagram of forces on the stabilizer.